CIVIL ENGINEERING JOURNAL

Article no. 19

THE CIVIL ENGINEERING JOURNAL 2-2025

CASE STUDY: ROCKFALL MITIGATION AT A HIGHWAY SLOPE IN SUICHUAN COUNTY, CHINA

Shuisheng Yang[1], Shalu Huang[1], Zhibin Tian[1] and Wanhao Yu[2]

1. *Jiangxi Provincial Highway Research and Design Institute Co., Ltd, Nanchang, 330002, Jiangxi, China*
2. *School of Civil Engineering, Sichuan University of Science & Engineering, Zigong, 643000, Sichuan, China; 1203945563@qq.com*

Received: *02.12.2024*
Received in revised form: *15.04.2025*
Accepted: *17.06.2025*

ABSTRACT

Conducting proper stability analysis of potential rockfall hazards and implementing appropriate prevention measures are crucial for ensuring highway safety. This study investigated a rock slope along the G105 National Highway in Suichuan, Jiangxi, China. The stability of the slope was evaluated through a combination of theoretical analysis and field investigation. The slope is stable under normal conditions but transitions to a state of partial instability or instability during extreme weather events or seismic activities, necessitating protective measures. To assess the risk of rockfall, a Rock-fally simulation was conducted. The deposition distribution, kinetic energy, translational velocity, and bounce height of rocks with varying volumes during the fall were simulated. The kinetic energy of rockfall is primarily influenced by the volume of the rock mass, while translational velocity, bounce height, and deposition distribution are closely associated with the cross-sectional conditions. Based on the evaluation results, appropriate reinforcement measures were selected, and the slope was monitored using InSAR and automatic monitoring technologies. The combination of drone scanning, modeling, automated monitoring techniques, and InSAR technology effectively reduces uncertainties in risk assessment. Based on the evaluation results, the application of active energy-absorbing protection nets and other preventive measures were proposed, demonstrating a satisfactory protective effect. The case study will provide valuable engineering guidance for rockfall analysis and prevention on highway slopes.

KEYWORDS

Rockfall, Slope monitoring, InSAR, Prevention engineering

INTRODUCTION

In the densely populated regions, where land resources are scarce, buildings and pathways were constructed along the mountains to maximize the utilization of the land. Nevertheless, the utilization of the mountain area endanger the stability of the slopes, of which the susceptibility to collapse and rockfall incidents is high [1]. This issue is particularly evident along the G105 National Highway, especially in the Suichuan segment, Jiangxi, China. Which is characterized by a complex geological environment and unstable slopes. These slopes, especially in areas with high gradients and loose rock formations, are highly prone to rockfalls and landslides. Additionally, natural factors such as rainfall and seismic events can trigger further instability, posing a significant threat to traffic

safety. The complexities are inextricably of rock fall linked to factors such as the site-specific characterisitcs of rockfalls, a lack of history rockfall datasets, and the difficulties of quantifying rockfall stability in diverse risk-coupling scenarios [2-5].

In previous years, rockfall research was limited by the limitations of technology, and rockfall prevention was predominantly based on experience and empirical approaches. Practices such as retaining walls, drainage systems and slope reinforcement have been used to increase the stability of rocky slopes. Furthermore, rock removal and periodic slope inspections were essential to promptly identify potential risks. Later, empirical approaches proved effective in initial slope assessments. However, relying solely on these methods to prevent collapses and rockfalls, reliance has often resulted in suboptimal results. The main uncertainties are that predicting rock displacement trajectories at different locations is difficult, which is a crucial factor in assessing rockfall hazards [6-8]. Therefore, scholars focus on computational modeling and introduced numerical simulation methods to evaluate the slope stability and predict disaster occurrences. The objective was to predict high-risk zones and support decision-making in implementing protective measures. Currently, the most used software for rockfall simulation is Rocfall. It conducts analyses involving translational velocity, rebound height, kinetic energy, and debris distribution caused by rockfalls [9-11].

Numerical simulation methods overcome the disadvantages of empirical approaches. However, these methodologies are not immune to inherent limitations that significantly affect the accuracy and reliability of simulation results. The effectiveness of the numerical model depends on the quality of the input data. Building a reliable rockfall model requires an extensive compilation of geological parameters and comprehensive monitoring data. However, the spatial and temporal variability of geological factors presents challenges in achieving forecast accuracy. Rockfall monitoring is typically required, which includes Global Navigation Satellite Systems (GNSS) or inclinometers. Automatic monitoring methods can be used in tracking movements of individual blocks and offer a high frequency of data acquisition. However, the application is limited to the specific points on the rock slope, meaning difficult to obtain the comprehensive capture of slope deformative characteristics [12]. Consequently, critical data relating to regions of unstable slopes may be omitted during monitoring, resulting in deficiencies in the numerical model's slope assessment. The latest technology in slope monitoring is Interferometric Synthetic Aperture Radar (InSAR). Compared to conventional methods, InSAR offers advantages such as improved spatial resolution, resilience to interference, broad coverage and monitoring capabilities in all weather conditions [13]. With continuous advancements and practical applications, InSAR has demonstrated advantages in monitoring rockfalls, landslides, and catastrophic scenarios. However, InSAR also has limitations, for example, its spatial resolution may be inadequate to accurately detect small rockfalls or localized deformations. Furthermore, the specifics of the terrain and dense vegetation can obstruct the visibility of slopes, increasing the challenges faced in monitoring rockfall [14-16]. In summary, numerical simulation techniques have been significantly improved, as an alternative method to empirical methods. However, the uncertainties of both the numerical simulation and the empirical method largely arise from the uncertainties inherent in monitoring data [17]. Improving the reliability, comprehensiveness and effectiveness of monitoring data in the context of rockfall management will now be useful for assessing the stability of rock slope.

In light of these considerations, this study focuses on a rocky slope along National Road G105 in Suichuan County and evaluates automated monitoring techniques together with InSAR technology. The study combines UAV remote sensing, 3D modeling, automated monitoring and InSAR, forming a basis for slope stability surveillance. Data collection is used to analyze rockfall incidents across multiple rock volumes and profiles, examining movement trajectories, velocities, rebound heights, kinetic energies, and debris distribution. It proposes several fortification strategies, including active and passive networks, shelters, and hazard reduction methods [18-19]. Through InSAR and automated monitoring, a comprehensive surveillance regime is established for the rockfall-prone region, offering continuous all- weather data for early warnings. These preventative measures have proven to be effective in mitigating slope collapses and rockfall incidents, providing valuable engineering insights for rockfall prevention.

OVERVIEW OF THE ROCK SLOPE

The rocky slope is located next to the G105 National Highway in Suichuan County, Jiangxi Province. The rock formation on the right side of the highway appears as a steep cliff, indicating the potential for rockfall. The geological hazard associated with this slope is classified as high-level rockfall, located on the steep cliff to the right of the highway. Through a comprehensive field investigation, three specific regions that present an elevated rockfall risk were pinpointed and denoted as WY1, WY2, and the concave cavity Figure 1 and Table 1 illustrate the location and attributes of the rock mass at this location.

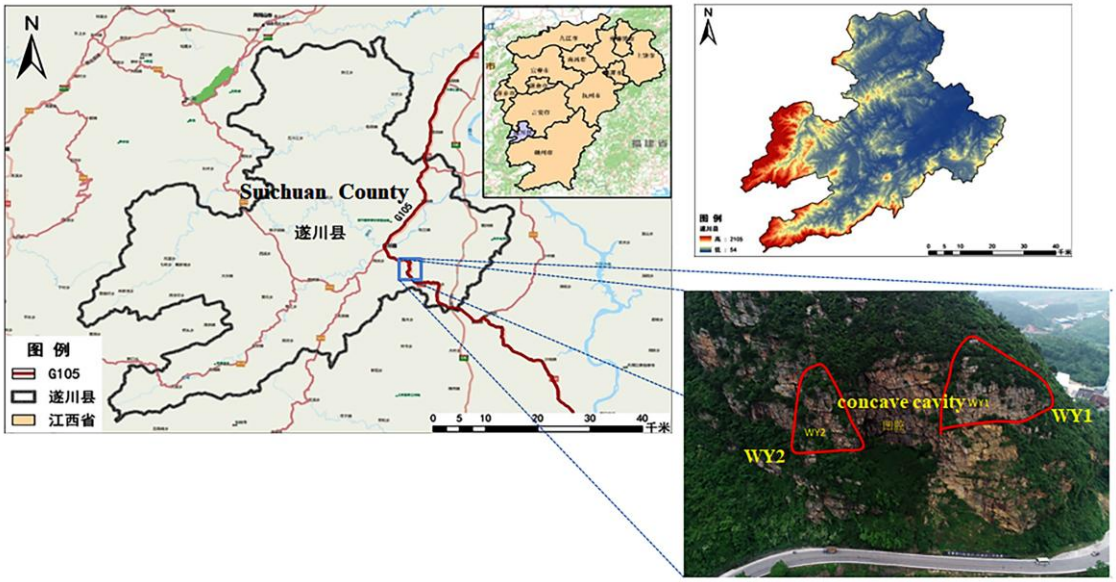

Fig. 1 - Location and illustration of the rockfall

Tab. 1 - Characteristics of regional rock masses

Characterization	WY1	WY2	Concave cavity
Height of the rock mass on the right	100-120m	150-170m	130-150m
Slope bottom features	The rock mass at the bottom of the cliff remains relatively intact with a higher vegetation cover, and scattered rock debris	The rock mass at the bottom of the cliff remains relatively intact with a higher vegetation cover, and scattered rock debris	Slope 50-65°, with a high vegetation cover and relatively intact rock mass, along with visible accumulations of rock debris.
Characteristics of rock mass cracks	70m from the ground, vertically extended, yielding 74°∠61°, about 30m in length and 50-80cm in width, with plant roots	70-75m from the ground, vertically extended, in line with WY1, length about 30m, width about 50-100cm	No obvious cracks were found, but gravity produced localized chipping and falling blocks

Dimensions of the bottom of the rock mass	Width about 36m, height about 30-35m, thickness about 7-10m, volume about 7560m^3	Width about 30m, height about 35-38m, thickness about 7.5m, volume about 3250m^3	

ROCK MASS STABILITY ANALYSIS

Qualitative Analysis

Based on field investigations and stereographic projection analysis, the rock mass structure in the study area is primarily controlled by the original bedding planes and two sets of high-angle joints (J1: 143°∠76°, J2: 25°∠88°). The bedding planes, with an orientation of 195°∠2°, form a typical counter-slope relationship with the slope surface (74°∠61°), and their dip angle is significantly lower than the critical friction angle required for sliding (typically >15°), effectively excluding the possibility of bedding-parallel slip.

In contrast, the two joint sets (J1 and J2) are densely developed (joint trace frequency > 5/m) and exhibit strong geometric compatibility with the slope surface. The angles between their strike directions and the slope orientation are approximately 69° and 49°, respectively, while their dip angles (76°–88°) are nearly parallel to the slope inclination (61°). This structural alignment facilitates tensile stress concentration along the joint planes under external loading, significantly reducing the tensile strength of the rock mass, and thereby promoting tensile failure along the joints.

Stability Calculation

According to site investigation, rockfall on this slope aligns with rotational landslide collapse. The center of gravity of the rock masses in WY1 and WY2 is positioned within the pivot point. Equation (1) is used for calculation when the stability is controlled by the tensile strength of the rear rock mass and the center of gravity of the hazardous rock mass lies within the overturning point. This equation is derived from the overturning stability calculation formula for hazardous rock slopes specified in the specification [20].

$$F = \frac{\frac{1}{2} f_{lk} \cdot \frac{H-h}{\sin\beta}\left(\frac{2}{3}\frac{(H-h)}{\sin\beta} + \frac{b}{\cos\alpha}\cos(\beta-\alpha)\right) + W \cdot a}{Q.h_0 + V\left(\frac{H-h}{\sin\beta} + \frac{h_w}{3\sin\beta} + \frac{b}{\cos\alpha}\cos(\beta-\alpha)\right)} \quad (1)$$

Here's the meanings of the parameters:

f_{lk}--- the standard tensile strength of the unstable rock mass (kPa), determined by multiplying the standard tensile strength of the rock by a reduction coefficient of 0.40;

h--- Depth of the rear edge crack (m);

h_w--- Water filling height of the rear edge crack (m);

h_0--- Vertical distance from center of gravity to tipping point (m);

H---Vertical distance from the upper end of the rear edge crack to the lower end of the unpenetrated segment (m);

W--- Self-weight of rock mass;

Q--- Seismic force(kN/m);

V--- Pressure of fractured water (kN/m);

a---Horizontal distance from the barycenter of mass of the unstable rock mass to the overturning

point (m);

b---Horizontal distance from the lower end of the unpenetrated segment of the rear edge crack to the overturning point (m);

α---Angle (°) between the contact surface of the unstable rock mass and the foundation. It takes a positive value when the rock mass is outwardly inclined and a negative value when inwardly inclined;

β---Angle (°) of the rear edge crack.

The inherent density of the rock is assumed to be 24 kN/m³, while the saturated density is set at 24.5 kN/m³. The tensile strength is estimated to be 400 kPa. Three distinct scenarios are considered for the calculations: the existing condition, the rainstorm condition and the seismic condition. For the existing condition, the calculations are based on the state observed during the investigation period, accounting only for the self-weight of the rock mass. In rainstorm conditions, the calculations take into account both the self-weight of the rock mass and the hydrostatic pressure within the fissures induced by heavy rainfall. This pressure, calculated using the hydrostatic pressure formula, is applied to the fracture surfaces and incorporated into the driving force generated by the self-weight of rock mass to assess the potential for sliding under heavy rainfall. Duri this scenario, the water level is presumed to range from 1/3 to 1/2 of the fissure depth. In the seismic condition, the calculations encompass the self-weight of the rock mass, seismic forces, and the influence of fissure water pressure. For seismic conditions, seismic inertial forces in both horizontal and vertical directions—derived from the product of the weight of rock mass and the seismic acceleration—are introduced to simulate earthquake-induced disturbances. In this scenario, the total driving force or adverse load is composed of the self-weight of rock mass, seismic inertial forces, and fracture water pressure. This total force is then compared with the resisting force, which includes cohesion and frictional resistance, to calculate the factor of safety. The stability outcomes are presented in Table 2, adhering to the guidelines delineated in the relevant standards for rock stability assessment [20].

Tab. 2 - Calculation results of rock mass stability

Rock mass number	Destruction mode	Working condition	Stability coefficient *Fs* of rock mass	Prevention and control safety level	Stability evaluation
WY1	Tilting type	Current conditions	3.12	Secondary	Stable
		Rainstorm condition	1.19		Unstable
		Seismic conditions	0.89		Unstable
WY2	Tilting type	Current conditions	2.85	Secondary	Stable
		Rainstorm condition	1.26		Approximately stable
		Seismic conditions	0.96		Unstable

The aforementioned results collectively suggest that the rock mass currently maintains a condition ranging from stable to moderate stability, meaning that the safety factor is not high, but still greater than 1.0. However, this state changes from a state of moderate stability to potential instability during rainstorm conditions, and changes to a fully unstable state during seismic events. Under such a circumstance, this could lead to disruptions in daily transportation or complete road closures when a storm or earthquake hits this area.

ROCKFALL SIMULATION

To accurately model rockfall behavior during descent, a detailed understanding of its complex influencing factors is required. To support data collection, fixed aerial control points were set up at the slope site, and an unmanned aerial vehicle (UAV) was used to capture images of the hillside rock mass. Based on these images, a 3D model of the slope was generated, as shown in Figure 2. The slope was divided into 29 sections from left to right for detailed analysis.

In model construction, appropriate values for parameters including slope slip coefficients, roughness, tangential damping coefficients, rockfall geometric attributes, rock dimensions, and density are selected based on data collected from field monitoring. The ensuing analysis that follows provides information on the distribution of rockfall stopping points across various slope cross-sections, along with assessments of kinetic energy, translational speed, and rebound height.

In Rock-fally simulations, rockfall modeling can intuitively illustrate the movement trajectories and impact locations of falling rocks, aiding in the assessment of risk zones and the effectiveness of protective measures. It offers advantages such as operational flexibility, low cost, and high repeatability. However, its strong dependence on input parameters and the simplifications inherent in the modeling process may lead to deviations from real-world conditions. Therefore, when applying such simulations, it is essential to incorporate field data and set parameters appropriately to enhance the reliability of the results.

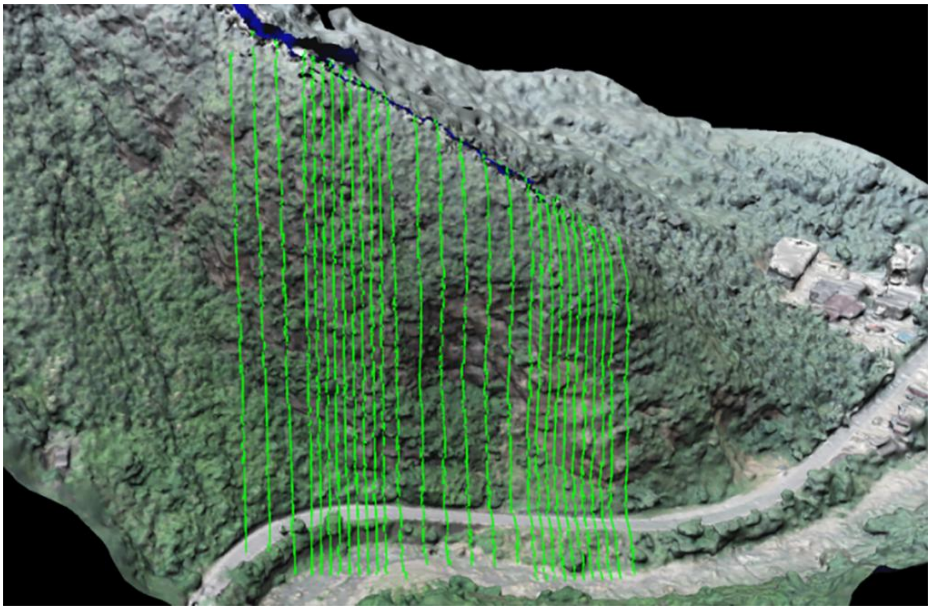

Fig. 2 - Location of simulated characteristic cross-section of slope

Three main cross-sections have been chosen for rockfall analysis, employing Rockfall software. To identify the influence of rocks with varying volumes, simulations have been carried out using rocks with dimensions of 5m³ and 10m³. The specific cross-sections and simulation models employed are illustrated in Figure 3. The material parameters of the slope in the simulation at three cross-sections are defined as bedrock outcrops, where the coefficient of normal restoration is set to 0.35, the coefficient of frictional restoration is set to 0.85, and the friction angle is set to 30.

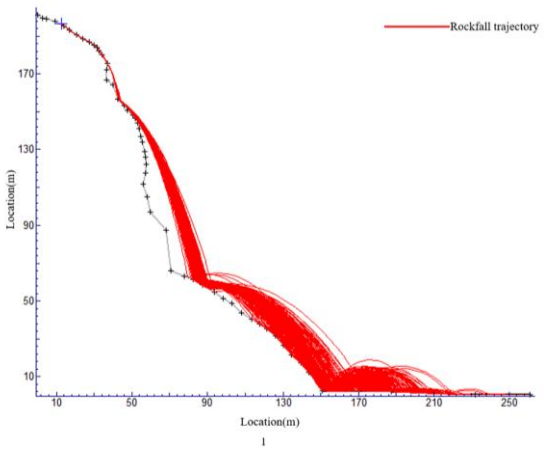

（a）Dimensions of 5m³ in section 1

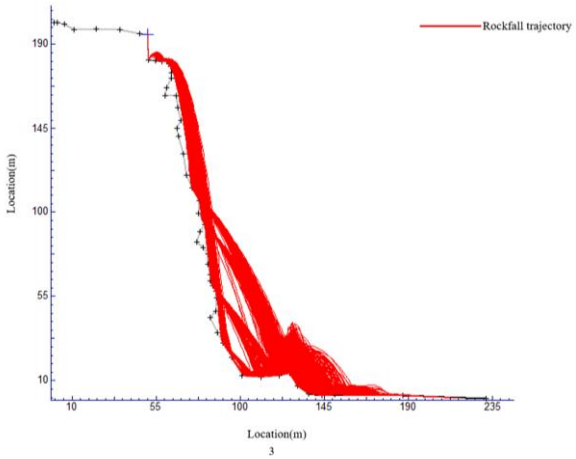

（e）Dimensions of 5m³ in section 3

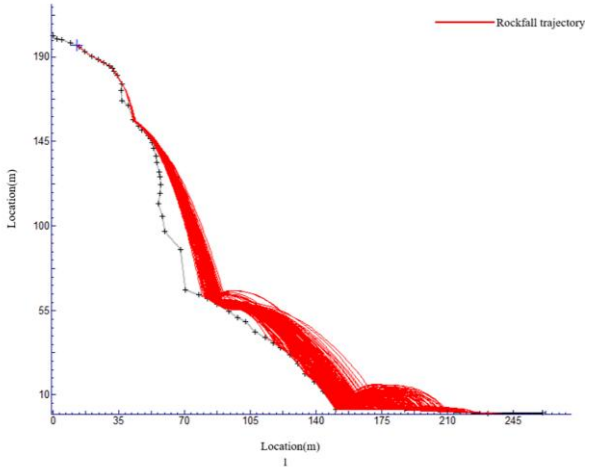

（b）Dimensions of 10m³ in section 1

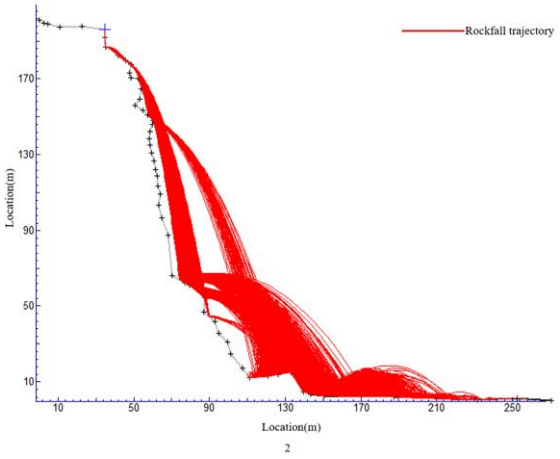

（d）Dimensions of 10m³ in section 2

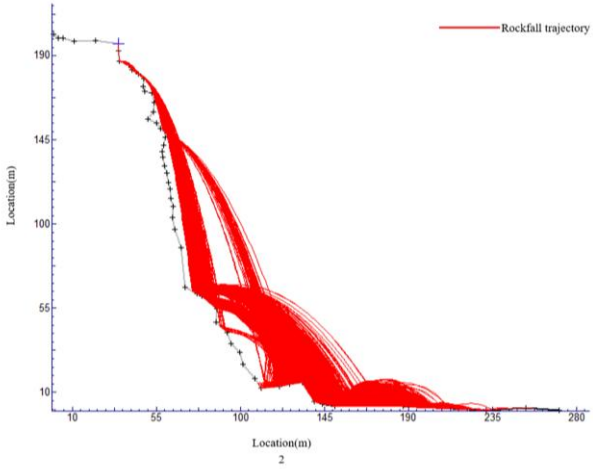

（c）Dimensions of 5m³ in section 2

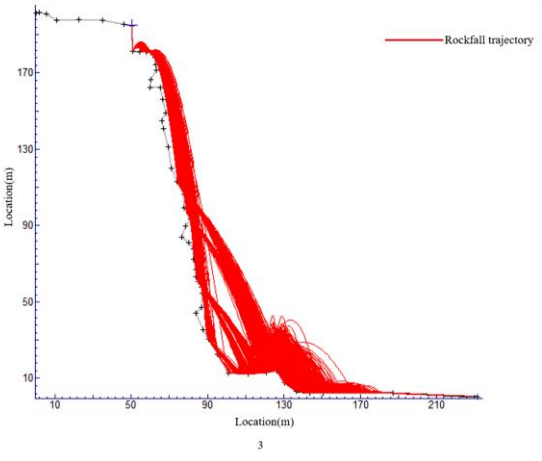

（f）Dimensions of 10m³ in section 3

Fig. 3 - Cross section rockfall trajectory map motion

In the Rocfall software simulation for the most representative sections, the falling rocks are initially set at a velocity of 0 m/s, with the final velocity likewise set at 0 m/s. The initial rotational velocity is also established at 0 m/s. The simulation is conducted over 1000 iterations for each

section, allowing for a comprehensive statistical analysis of rockfall incidents. The rock density employed in the simulation is specified at 2500 kg/m³. The normal and tangential restitution coefficients are predominantly contingent on the attributes of the surface of slope covering and vegetation. The values for these coefficients have been derived from the geotechnical investigation papers [21-22].

Model Calculation Results

(1) The influence of Deposition

The simulation results are based on probabilistic statistical analysis. The corresponding number of simulated rockfall sections is shown in Figure 4. In Section 1, for falling rock volumes of 5m³, a portion of them comes to rest within the range of 10-40m, with the highest count of falling points noted at 13m, totaling 579. When the volume of falling rocks increases to 10m³, some of them accumulate within 10-30m, and the count at 13m is 597.

In Cross-section 2, for a rock volume of 5m³, deposition is predominantly observed between 150-210m, with the peak number of points recorded at approximately 205m, amounting to 132. With a rock volume of 10m³, the maximum number of points is observed between 190-220m, reaching a peak of 119 at 211m.

In Cross-section 3, the rock volume is it 5m³, the points of deposition are concentrated around 152m, with over 227 points. With a rock volume of 10m³, the maximum number of points is observed between 140-170m, reaching a peak of 250 at 153m.

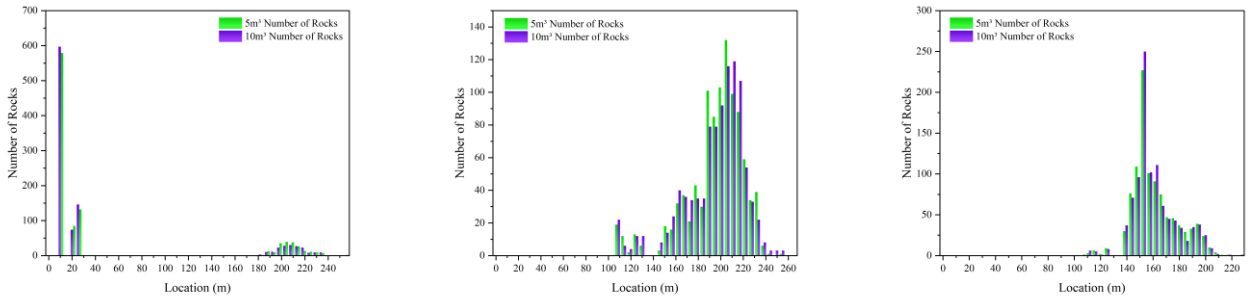

（a）Section 1　　（b）Section 2　　（c）Section 3

Fig. 4 - Number of falling rocks chart

Based on the statistical analysis of rockfall across the three cross-sections, it is evident that the change in rock volume has a relatively minor effect on deposition distribution, while the geometric and structural characteristics of the slope sections play a more dominant role. Among the three, Cross-section 2 exhibits the highest overall hazard coefficient, as indicated by the greater number and broader spread of rockfall deposition points. This suggests more intense and frequent rockfall activity in that area.

In contrast, although Cross-section 3 has the lowest overall hazard coefficient, it presents the most severe risk of road encroachment. The reason lies in the proximity of its deposition zone to the roadway—many rockfall points are located very close to, or even directly on, the road surface. This concentrated deposition near the road significantly increases the likelihood of traffic obstruction or accidents, even with fewer total events. Therefore, despite its lower general hazard, Cross-section 3 poses a more immediate and tangible threat to road safety. As such, it is strongly recommended to prioritize the implementation of protective measures along this section to mitigate the risk of road blockage caused by rockfall.

(2) The influence of Kinetic Energy

The total kinetic energy diagram is shown in Figure 5. It is evident that in Cross-section 1, the maximum kinetic energy escalates to 5,500 kJ when the rock volume is 5m³, and surges to 11,000

kJ when the volume expands to 10m³. In Cross-section 2, the maximum kinetic energy registers at 7,400 kJ for a rock volume of 5m³, and reaches 15,000 kJ for a volume of 10m³. In Cross-section 3, the highest kinetic energy is recorded at 7,100 kJ for a rock volume of 5m³, and ascends to 1,4000 kJ for a volume of 10m³. The curves illustrating the rise in kinetic energy gradually ascend to a peak before descending, a pattern that closely mirrors the motion characteristics of rockfall during the collapse. With the assumption of consistent variables, such as cross-section attributes, it becomes evident that rock volume exhibits a distinct positive correlation with kinetic energy.

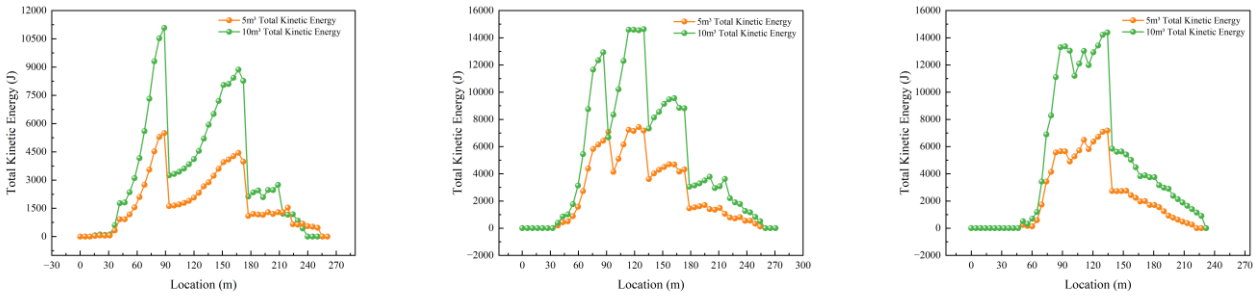

（a）Section 1　　（b）Section 2　　（c）Section 3

Fig. 5 - Total kinetic energy diagram

An excess of kinetic energy can cause damage upon the road infrastructure, posing a substantial threat to lives and property. A thorough analysis of rockfall kinetic energy serves as a reference for the choice of protective structures, ultimately resulting in an effective reduction in the costs associated with engineering measures.

(3) The influence of Translational Velocity

The horizontal velocity of falling rocks at different cross-sections under different volumes is shown in Figure 6. The rockfall translational velocities as rocks descend from elevated positions, the conversion of potential energy to kinetic energy induces alterations in velocity. These variations in velocity serve as indicators of the roughness of the slope throughout the motion, facilitating an analysis of slope safety.

It is evident that in Cross-section 1, the maximum translational velocity attains 46 m/s for a rock volume of 5 m³, and escalates to 47 m/s for a volume of 10 m³. In Cross-section 2, the utmost translational velocity is recorded at 53 m/s for a rock volume of 5 m³, and slightly higher at 55 m/s for a volume of 10 m³. In Cross-section 3, the highest translational velocity is noted at 55 m/s for a rock volume of 5 m³, and it marginally reduces to 55 m/s for a volume of 10 m³.

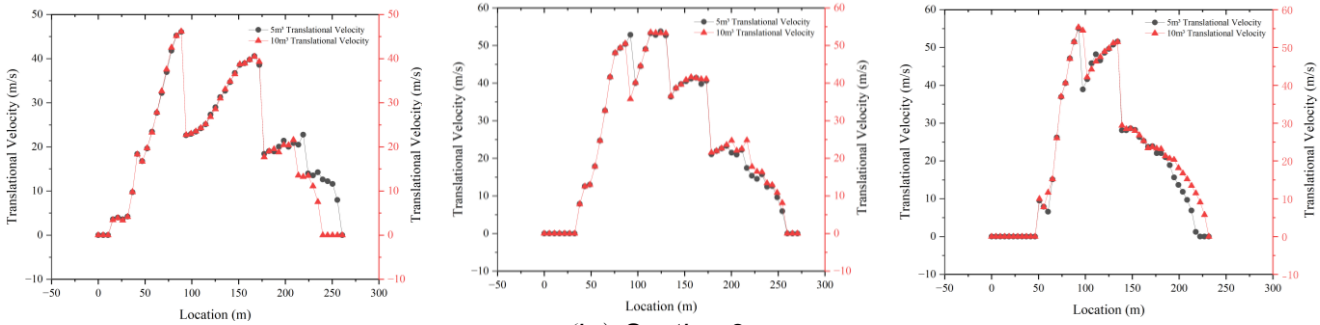

（a）Section 1　　（b）Section 2　　（c）Section 3

Fig. 6 - Translational velocity of falling rocks

The analysis of peak translational velocities leads to the conclusion that the alteration in rock volume exerts minimal influence, while the characteristics of the cross-section play a more important role in determining translational velocity. Specifically, a higher starting point for the rockfall results in

greater translational velocity.

The sequence of peak translational velocities, from highest to lowest, aligns with the analysis of rockfall deposition points, Cross-section 1 exhibits the highest velocity, followed by Cross-section 2, and then Cross-section 3. This sequence further underscores the urgency for mitigation measures to ensure the road safety from the rockfall hazards posed by this slope.

(4) The influence of Bounce Height

The rockfall bounce height corresponding to the section taken is shown in Figure 7. Throughout the descent of rockfall, the rocks may experience multiple rebounds upon striking various surfaces. Each bounce has the potential to cause damage to the slope and lead to a dissipation of energy.

It is evident that in Cross-section 1, the maximum bounce height reaches 53m for a rock volume of 5m³ and 55m for a volume of 10m³. In Cross-section 2, the maximum bounce height attains 72m for both rock volumes (5m³ and 10m³). In Cross-section 3, the highest bounce height is measured at 65m for a rock volume of 5m³ and 66m for a volume of 10m³. The examination of bounce height across different cross-sections indicates that rock volume has a marginal effect on bounce height, whereas the characteristics of the cross-section exert a more substantial influence.

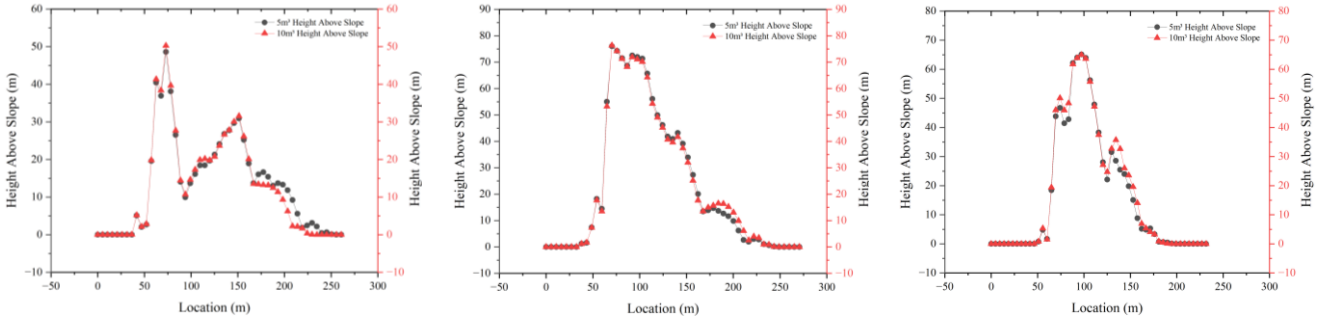

（a）Section 1　（b）Section 2　（c）Section 3

Fig. 7 - Rockfall rebound height chart

In summary, the distribution of rockfall deposition, translational velocities, and bounce heights are briefly determined by cross-section itself, such as initial elevation and slope friction coefficient. Meanwhile, rockfall kinetic energy is predominantly influenced by rock volume. The rockfall simulations and subsequent analysis affirm that in the selected three representative cross-sections, the maximum bounce height is 72m, the peak translational velocity is 55m/s, and the highest kinetic energy is 15,000 kJ, all of which are observed in Cross-section 2. This analysis concurs with prior calculations and field surveys, indication that rockfall poses a great threat to the use of the road.

DEFORMATION MONITORING BASED ON INSAR

To evaluate the deformation of the rock slope in the Suichuan segment of the G105 National Highway, the analysis made use of both D-InSAR and SBAS-InSAR methodologies for comprehensive area monitoring. A total of 15 ascending orbit data scenes sourced from Sentinel-1A were selected and subsequently processed. The study adopted the wide-swath interferometric mode with VV polarization, generating Single Look Complex data in Level-1. The chosen mode was Scan SAR-interferometric wide-swath (IW), covering a time duration of 168 days. InSAR technology offers significant cost advantages and spatial continuity for large-scale slope monitoring, with its millimeter-level accuracy meeting the early warning requirements for highway slopes. Compared to traditional methods, the automated InSAR system enhances data acquisition efficiency by approximately six times and is not limited by terrain accessibility. While the GNSS reference station provides a point monitoring accuracy of ±2 mm, its deployment density is limited; total stations, though capable of sub-millimeter precision, require manual periodic measurements, and data acquisition may be interrupted by extreme weather conditions, such as heavy rainfall. The construction cost of traditional monitoring networks (GNSS combined with total station) is approximately USD 36,000/km, while the cost of InSAR in this study is only 17% of the traditional method. Particularly in high and steep slope areas, where manual monitoring poses safety risks, InSAR technology demonstrates significant advantages.

D-InSAR

Differential Interferometric Synthetic Aperture Radar (D-InSAR) technology primarily needs integrating external Digital Elevation Model (DEM) data to remove the terrain phase from the interferogram derived from InSAR. At present, three primary D-InSAR techniques are commonly employed: two-pass, three-pass, and four-pass interferometry. Among them, the two-pass interferometric method is regarded as the most reliable due to its relatively simple implementation and high accuracy.

Following the D-InSAR analysis, the Sentinel-1A data were processed with two-pass interferometric method. This led to the generation of a surface deformation map, which unveiled non-uniform ground deformation along the entirety of the road. The severely impacted regions primarily cluster in the northern section, showcasing surface uplift with the maximum deformation measuring 0.219 m. In comparison, the deformation in the southern section is slightly lesser than that in the northern section, with most deformations falling below 0.06 m. Within the central urban area, the road segment indicates subsidence of approximately less than 0.08 m.

SBAS-InSAR

SBAS-InSAR stands for Small BAseline Subset InSAR, through the combination of a substantial amount of SAR data, a series of differential interferograms with short spatial baselines can be derived. This effectively avoids spatial decorrelation, enhancing the accuracy of the deformation analysis.

Following the two-pass interferometric processing of the Sentinel-1A data, the average deformation rates along the G105 Suichuan section were computed. The overall deformation along the road corridor is relatively modest, with the majority of regions displaying an annual average deformation rate of approximately ±50mm/year. The regions experiencing severe deformation are primarily concentrated in the northeastern section, where the maximum subsidence rate reaches 50mm/year. Deformation rates in the southern section generally remain below 30mm/year, while in the central urban area, the road segments undergo minimal deformation, with an average deformation rate of around ±10mm/year.

For a more detailed analysis of the deformation characteristics in the high-altitude collapse areas along the G105 Suichuan section, seven key points of interest were selected. These points encompass locations along the road alignment and within the range of the slope collapse, as shown in Figure 8.

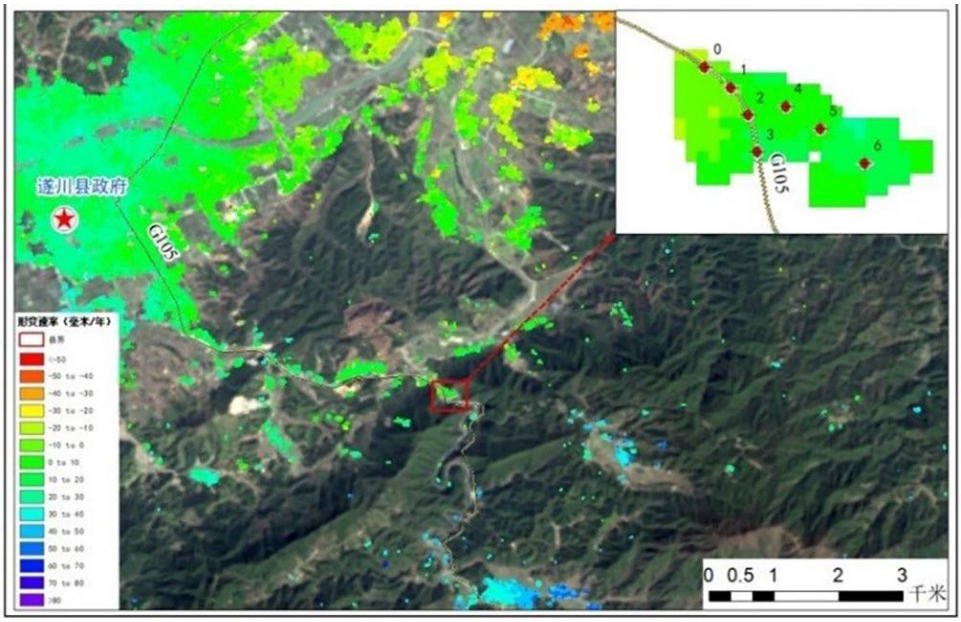

Fig. 8 - Deformation rate diagram of the collapse points of Suichuan section G105 during the monitoring period

Through monitoring the deformation of high-risk collapse points, all seven monitoring locations exhibited distinct deformation behaviors during the entire observation period. Generally, points 0 and 1 showed noticeable subsidence, while the remaining five points exhibited slight uplift.

Among these, point 3 demonstrated the greatest subsidence, reaching approximately 20 mm between April 8 and April 20. Point 1 followed with a subsidence of 13 mm between July 1 and August 6. Point 2 remained relatively stable, with fluctuations confined within 8 mm throughout the monitoring period, although a significant uplift was observed after August 6.

The deformation behavior at all monitoring points exhibited fluctuating patterns, which may indicate episodic instability, potentially linked to anthropogenic activities. Several monitoring points exhibited synchronized deformation trends, with abrupt subsidence or uplift occurring at specific intervals. These significant deformation events underscore the importance of implementing timely protective measures to ensure the safety of both vehicular traffic and pedestrians in the affected areas.

MITIGATION MEASURES

Guided by theoretical calculations and assessments conducted through simulation software, this study proposes the implementation of an actively controlled energy dissipation net in conjunction with a rockfall protection system as well as the tunnel construction. In the case of rocks WY1 and WY2, primarily due to their substantial volume and the emergence of unloading cracks at the rear edge, it is advisable to initiate manual rock extraction as the preliminary measures. Furthermore, a primary energy dissipation net will be strategically installed beneath the rocks. The lower section of the net will feature an open design, while the remaining sections will be closed. This will result in a total length of 260 meters and an average height of 155 meters. The protective area will encompass 40,300 square meters.

In the construction of the tunnel, an open-cut method will be employed, strategically positioned at the most severely affected areas. The tunnel will take the form of an integral, single-aisle, two-way driving structure, spanning a total length of 210 meters. The design takes into account a 2-meter diameter rock block falling from a height of 100 meters, resulting in an impact force of approximately 838kN/m. To support the outer side of the tunnel, pile foundations will be employed, while the top will be filled with crushed stones at a slope ratio of 50% [23]. In order to ensure the rationality and feasibility of the proposed protection measures, a preliminary cost estimation has been conducted. The estimated investment includes the following components: Manual removal of unstable rocks (WY1 and WY2); Energy dissipation net (260m × 155m, covering 40,300 m²); Tunnel construction (210m, open-cut method); Pile foundations; Backfill and slope treatment; Safety monitoring system. The total estimated cost is approximately USD 2.57 million. Considering potential geological uncertainties and implementation risks, it is recommended to set aside an additional 10% contingency, bringing the overall estimate to about USD 2.83 million. These investments are considered necessary and cost-effective, given the potential consequences of rockfall hazards in the project area.

Automated Monitoring

To monitor the potential rockfalls during and post the construction phase, a comprehensive combination of automated monitoring techniques will be deployed. This array includes the monitoring of surface deformation, precipitation levels, rock tilt angles, fractures in the rock, and on-site conditions of the mountain. The primary monitoring method will need the use of GNSS satellite positioning to track the absolute displacement of the slope. For fracture monitoring, points will be strategically installed at locations exhibiting instability and pre-existing cracks.

Moreover, rain gauges will be positioned at higher sections of the slope, isolated from the influence of the surrounding environment. Wireless tilt monitors will provide real-time observations of rock tilt variations. In the event that the tilt of the rock exceeds the predetermined warning threshold, timely alerts will be issued. Video surveillance cameras will be strategically stationed in

open and unobstructed areas to provide panoramic views of potential collapse and rockfall zones, enabling real-time and comprehensive monitoring. The layout of the monitoring stations and the monitoring site is depicted in Figure9.

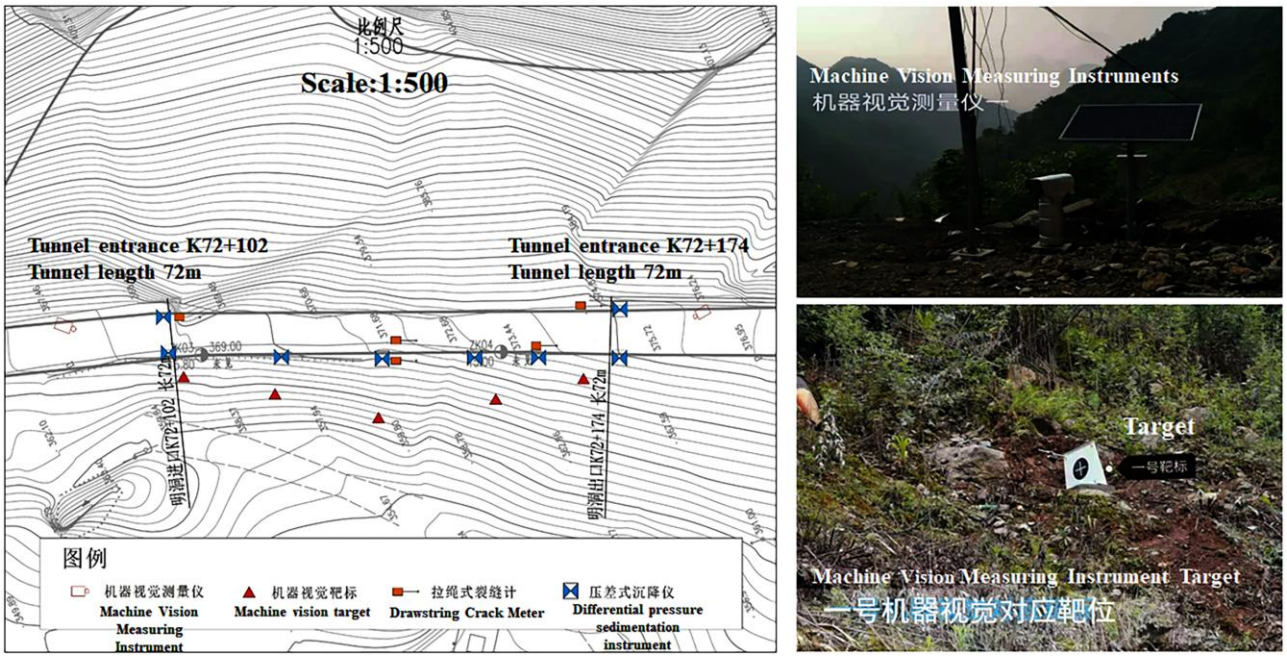

Fig. 9 - Layout of monitoring stations and monitoring sites

The post-construction monitoring outcomes reveal that the machine vision measuring instrument recorded the highest cumulative horizontal displacement at 9.64 mm, while the ground exhibited a vertical displacement of -9.68 mm. The settlement inclinometer detected a maximum cumulative change of -8.33 mm. In the x-direction inclinometer, which comprises one reference point, one turning point, and ten valid points, the maximum cumulative change during the monitoring period is -0.21°. In the y-direction inclinometer, the maximum cumulative change is -0.18°. The rope extensometers registered a maximum cumulative change of 0.48 mm.

Based on the results of automated monitoring, the monitoring system demonstrates relative stability. The measured values at various monitoring points in the slope stabilization project display minor variations, indicating that the slope is in a stable condition. Additionally, no ongoing expansion of cracks in the tunnel is observed, and there are no significant signs of uneven settlement in the tunnel foundation.

CONCLUSION

This study focuses on a rocky slope in the Suichuan segment of the G105 National Highway, conducting a qualitative analysis of the rock mass in the area. A three-dimensional representation of the slope is constructed using unmanned aerial vehicle (UAV) scanning. Rocfall software then analyzes the translational velocity, rebound height, kinetic energy, and deposition distribution for varying rockfall volumes. Additionally, slope stability is monitored through the integration of InSAR and automated monitoring technologies. By combining traditional slope stabilization methods with advanced intelligent monitoring approaches, this study effectively prevents and controls slope instability, leading to the following conclusions.

The rocks WY1 and WY2 on the slope remain stable under normal conditions, showing slight instability during heavy rainfall and becoming prone to instability during seismic events. The slope is particularly vulnerable to high-level collapses, with potential block falls and large-scale collapses along structural planes. Proposed measures, such as active energy dissipation nets, manual rock

removal, and strategic tunnel engineering, effectively control and prevent rockfalls.

Simulation results from Rocfall software show a strong positive correlation between the kinetic energy of rockfall and the volume of falling rocks. Meanwhile, translational velocity, rebound height, and deposition distribution are primarily influenced by cross-sectional conditions, such as the height of the falling points and friction coefficients on the impact surface, with no significant relationship to the rockfall volume. The combination of UAV scanning, automated monitoring, and InSAR technology reduces uncertainties in slope risk assessment, making the monitoring data more precise and reliable.

In conclusion, the comprehensive integration of various techniques in this study has been instrumental in assessing and mitigating rockfall risks on the designated slope. The insights gained from this research will provide valuable guidance for similar engineering projects addressing rockfall risks.

ACKNOWLEDGMENTS

This work was Supported by the Development and Application of Landslide Surface Deformation Monitoring System based on High-precision Beidou Technology (No. 2022H0030).

REFERENCES

[1] Zou D, Zheng H., 2005. Fast lagrangian method and its applications in slope stability analysis [J]. Mining Research and Development. 2005(10). https://doi.org/10.3969/j.issn.1005-2763.2005.05.026

[2] Glade T., 2003. Vulnerability assessment in landslide risk analysis. Die Erde 134:121–138.

[3] Crosta G B, Agliardi F., 2004. Parametric evaluation of 3D dispersion of rockfall trajectories. Natural Hazards and Earth System Sciences 4(4):583–598.

[4] Michoud C, Derron M H, Horton P, Jaboyedoff M, Baillifard F J, Loye A, Nicolet P, Pedrazzini A, Queyrel A., 2012. Rockfall hazard and risk assessments along roads at a regional scale: example in Swiss Alps. Natural Hazards and Earth System Science 12(3):615–629.

[5] Frattini P, Crosta G B, Carrara A, Agliardi F., 2008. Assessment of rockfall susceptibility by integr ating statistical and physically-based approaches. Geomorphology 94(3–4):419– 437. https://doi.org/10.1 016/j.geomorph.2006.10.037

[6] Azzoni A, La Barbera G, Zaninetti A., 1995. Analysis and prediction of rockfalls using a mathematical model. International Journal of Rock Mechanics and Mining Sciences & Geomechanics Abstracts 32(7):709–724. https://doi.org/10.1016/0148-9062(95)00018-C

[7] Agliardi F, Crosta G B., 2003. High resolution three-dimensional numerical modelling of rockfalls. International Journal of Rock Mechanics and Mining Sciences 40(4):455–471. https://doi.org/10.1016/S1365-1609(03)00021-2

[8] Frattini P, Crosta G B, Agliardi F., 2012. Rockfall characterization and modeling. In: Clague JJ, Stead D (eds) Landslides types, mechanisms and modeling. Cambridge University Press, Cambridge, pp 267–281, ISBN: 978-1-107-00206-7. https://doi.org/10.1017/CBO9780511740367.023

[9] Dorren, Luuk K A., 2003. A review of rockfall mechanics and modelling approaches [J]. Progress in Physical Geography, 2003, 27(1).

[10] Giani G P, Giacomini A, Migliazza M, et al., 2004. Experimental and Theoretical Studies to Improve Rock Fall Analysis and Protection Work Design[J]. Rock Mechanics & Rock Engineering, 2004, 37(5):369-389.

[11] Lan H, Martin C D, Zhou C, et al., 2010. Rockfall hazard analysis using LiDAR and spatial modeling[J]. Geomorphology, 2010, 118 (1–2):213-223. https://doi.org/10.1016/j.geomorph.2010.01.002

[12] Zhang Q, Huang G W, Yang C S.,2017. Precision space observation technique for geological hazard monitoring and early warning[J]. Acta Geodaetica et Car-tographica Sinica, 2017,46 (10): 1300-1307. https://doi.org/10.11947/j. AGCS.2017.20170453.

[13] Zhu J J, Li Z W, Hu J.,2017. Research progress and methods of InSAR for deformation monitori ng[J]. Acta Geodaetica et Cartographica Sinica, 2017, 46(10): 1717-1733. https://doi.org/10.11947/j.AG

CS.2017.20170350
[14] Zhu J J, Hu J, Li Z W, et al.,2022. Recent progress in landslide monitoring with InSAR[J]. Acta Geodaetica et Cartographica Sinica, 2022 ,51(10) :2001- 2019.
[15] FERRETTI A, PRATI C, ROCCA F.,2001. Permanent scatter-ers in SAR interferometry[J]. IEEE Tr ansactions on Geo-science and Remote Sensing,2001, 39(1): 8-20. https://doi.org/10.1109/IGARSS.199 9.772008
[16] B Y K A, B Z L, A C Z, et al.,2023. InSAR monitoring of creeping landslides in mountainous regions: A case study in Eldorado National Forest, California[J]. Remote Sensing of Environment, 258. https://doi.org/10.1016/j.rse.2021.112400
[17] Nadim F, Einstein H, Roberds W., 2005. Probabilistic stability analysis for individual slopes in soil and rock. In: Hungr O, Fell R, Couture R, Eberhardt E (eds) Landslide risk management. Taylor and Francis, London, pp 3–26. https://doi.org/10.1201/9781439833711-6
[18] Gharpure A D, Khan S S., 2022. Rock Fall Prevention by Innovative Products and Technologies [J]. gndec.ac.in, 2022.
[19] Bokati N, Dahal R, Acharya I, et al., 2020. Evaluation of rock fall analysis and suitable protection measures in siddhababa section along siddhartha highway[J].2020.
[20] (DB50/143-2003) Geological Hazard Prevention and Control Engineering Survey Specification [S].
[21] Bozzolo Dopamine R., 1986. Simulation of Rock falls down a Valley side[J]. Acta Mech,1986,63:113-130. https://doi.org/10.1007/BF01182543
[22] Day R W., 1997. Case studies of rockfall in soft versus hard rock [J]. Environmental and Engineering Geoscience,1997,3(1)：133-140. https://doi.org/10.2113/GSEEGEOSCI.III.1.133
[23] (JTG/T D70-2010) Design Rules for Highway Tunnels [S].